Deutscher Luft- und Raumfahrtkongress 2016
DocumentID: 420124

FLIGHT MECHANICS MODEL FOR SPANWISE LIFT AND ROLLING MOMENT DISTRIBUTIONS OF A SEGMENTED ACTIVE HIGH-LIFT WING

J.H. Diekmann, DLR, Institute of Flight Systems
38108 Braunschweig, Germany
D. Keller, DLR, Institute of Aerodynamics and Flow Technology
38108 Braunschweig, Germany
E. Faez, TU Hamburg Harburg, Institute of Air Transportation Systems
21079 Hamburg, Germany
R. Rudnik, DLR, Institute of Aerodynamics and Flow Technology
38108 Braunschweig, Germany
V. Gollnick, DLR, Institute of Air Transportation Systems
21079 Hamburg, Germany

Abstract

In this study the aerodynamics of wings using an active high-lift system are investigated. The target is the flight mechanical description of the spanwise forces and resulting moments and the influence of the active high-lift system to their distribution. The high-lift system is a blown flap system divided into six segments per wing. Each segment is assumed to be individually controlled, so the system shall be used for aircraft control and system failure management. This work presents a flight mechanical model for fast-time simulation of flight dynamics, which has been derived from high-fidelity CFD results. An assessment of single segment system failures will be presented including recommendations for compensation of either lift or rolling moment loss. For this investigation, the compensation is required to act at the same wing on which the failure appears. Thus, the potential for an increase of system reliability shall be proven. The results show that less performance investment is necessary to compensate the rolling moment of a failing segment instead of its lift. However, large performance increases for the remaining wing segments occur for some of the failure cases.

Nomenclature

B	Failure model area	-
C	Coefficient or derivative	-
$\tilde{C}_L$	Lift coefficient for segment failure	-
$C_{L,loc}$	Local lift coefficient	-
dC_L	Spanwise lift coefficient increment	-
c_{loc}	Local wing chord length	m
c_{MAC}	Wing mean aerodynamic chord length	m
C_μ	Jet momentum coefficient	-
$C_{\mu,loc}$	Local jet momentum coefficient	-
c_p	Pressure coefficient	-
E	Segment failure factor	-
F	Force	N
I	Mass inertia	kgm^2
$\hat{k}$	Mapping gradient for local jet momentum	-
k	Lift Gradient w.r.t. jet momentum	-
M	Mach number	-
m	Mass	kg
$\dot{m}$	Mass flow	kg/s
P	Jet momentum performance factor	-
p,q,r	Angular rates	°/s
$q_\infty, \bar{q}$	Dynamic pressure	N/m^2
S	Main wing area	m^2
u_k, v_k, w_k	Aircraft velocity (inertial frame)	m/s
v_{jet}	Fluid velocity	m/s
x,y,z	Aircraft position	m
Y, η	Dimensionless wingspan location	N
α	Angle of attack	°
Φ, Θ, Ψ	Aircraft attitude angles	°

Indices and Superscripts

c_μ	w.r.t. jet momentum coefficient
fl	Flap
i	Number of wing segment
j	Normalized wingspan coordinate
jet	Jet of the blowing system
L	Lift
l	Rolling moment
n	Number of jet momentum setting

Abbreviations

6-DOF	Six degrees of freedom
BLC	Boundary Layer Control
CC	Circulation Control
CFD	Computational Fluid Dynamics
DLR	Deutsches Zentrum für Luft- und Raumfahrt (German Aerospace Center)
IBF	Internally blown flaps
NASA	National Aeronautics and Space Administration
PrADO	Preliminary Aircraft Design and Optimization [tool]
SFB	Sonderforschungsbereich (Collaborative Research Center)
STOL	Short Take-off and Landing

1 Introduction

In the history of aircraft development for short take-off and landing (STOL) various active high-lift technologies have been put to the test [1]. A promising technology providing large lift increases for comparably small amounts of extra power, is to blow flaps with a thin airflow. Such systems, known as internally blown flaps (IBF), shall be the focus for this investigation. This work is related to the collaborative research center Sonderforschungsbereich 880 (SFB 880), in which a twin turbo-propeller engine powered aircraft design including blown single-hinged plain flaps is developed and investigated. The aim is to provide integral research up to the full aircraft level, combining expertise from research fields such as aerodynamics, flight mechanics, aircraft configuration, compressor technology and several more. The declared goal is to facilitate the integration of blown flaps in a civil transport type aircraft, in order to operate on small airfields. Such airfields, which already exist and often are located closely to urban areas, can be easily used to extend the transport infrastructure by point to point connections, to relieve large and highly frequented hubs.

The idea of combining the lift increasing effects of a propeller slipstream along the wing profile with a blown flaps system has been realized before. The NASA conducted a large research program for STOL aircraft starting in the mid fifties [2] with wind tunnel tests [3–5] and several prototypes. One of the investigated configurations, which is most comparable to the SFB 880 configuration, was the Lockheed Hercules NC-130B. In addition to its four turbo-propeller engines, it was equipped with two extra full size jet engines to provide pressurized air for blown flaps and control surfaces. The flight tests, which where conducted in the early 1960s, demonstrated the aircraft's remarkable abilities for slow flight and high-lift performance, but also revealed several challenges. Especially weight penalties, remarkably increased relative cost [6] and poor lateral as well as directional characteristics due to low directional damping and stability have been determined [7, 8]. The aircraft design of the SFB 880 tries to achieve similar flight performance without the described deficiencies by latest technologies and research in order to exploit the considerable potential of such high-lift technology combinations. The aircraft configuration design to achieve all these targets is performed by the preliminary aircraft design and optimization tool PrADO [9] incorporating all information about the various subsystems and influences provided by the different research fields of the SFB 880. For the iteratively calculated design, it delivers a full data set of basic aircraft information.

One of the research fields is the source of the necessary pressurized air. Therefore, small micro-compressors are developed within the collaborative research center, specially shaped for the application as a source for pressurized air [10]. They will be located in the wingbox close to the blown flaps as depicted in Figure 1. A possible

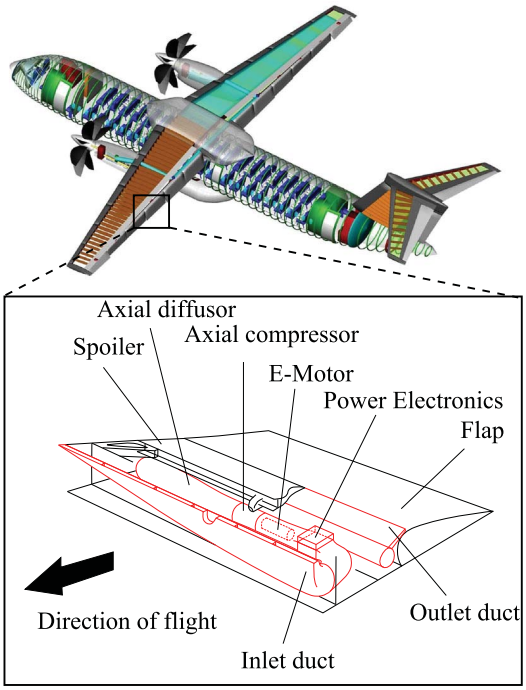

Figure 1: Cutaway drawing of the SFB 880 reference aircraft and active high-lift system integration [11]

measure to support the controllability in the lateral motion of the aircraft might be a multifunctional use of an active high-lift system. Multifunctional flaps have been investigated with several approaches. E.g. Sakurai et al. proposed a device based on single slotted flaps [12]. The aircraft design of the SFB 880 offers the chance to implement a similar system by differential blowing instead of flap deflections. The wing of the aircraft is separated into six segments per wing, each driven by a custom-

sized compressor. This offers several chances in terms of redundancy, but also creates new possibilities for differential control. Besides the influence on lift, a differential blowing can also generate rolling moments, which can be used for control or compensation. However, since the system depends on additionally generated air flows, it becomes sensitive to malfunction or failure, which need to be considered in requirements for reliability and safe operation. The impact of the resulting forces and moments and their compensation are important aspects in terms of hazard assessment. In order to investigate the multifunctional flap capabilities and to provide a failure assessment it is necessary to develop a flight mechanical model for the wings' spanwise aerodynamics. Therefore, a possible modeling approach and failure case management on the sub-model level will be subject of this work. In the following paper the focus exclusively lies on the aerodynamics of the flap system and excludes propeller slipstream effects. This is done in order to develop a universal understanding of the technology's potential. Certainly, further research effort will have to take the influence of the propeller slipstream into account.

2 Active High-Lift Aircraft Configuration

To gain a proper understanding of the underlying effect the used high-lift system is based on, the technology and the aerodynamic behavior will be explained. Figure 2 shows a sketch of the wing profile and how the blowing system can be implemented, based on results of research activities in the SFB 880 [13–16]. The special

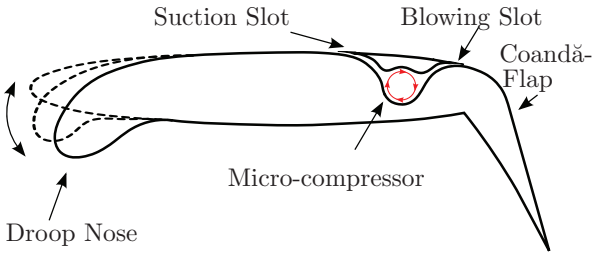

Figure 2: Schematic diagram of the SFB 880 wing profile and the active high-lift system integration

shape of the knee of the flap utilizes the Conadă effect, which describes the tendency of a thin highly energetic jet to follow a convex surface. This effect is used to keep the airflow attached to the flap surface even for large flap deflections at which the airflow would normally be separated. The state of the thin jet is usually described by the jet momentum coefficient C_μ, which relates the jet momentum to the dynamic pressure q_∞ and a reference area S.

$$C_\mu = \frac{\dot{m}_{jet} \cdot v_{jet}}{q_\infty \cdot S} \tag{1}$$

The lift increasing effect of the blown flap can be divided into two areas of efficiency. In the boundary layer control (BLC) area the jet and consequently the main wing wake are not fully attached to the flap. With increasing jet momentum, the separation is reduced. The effect is illustrated in Figure 3a and 3b. Once the flow is fully attached

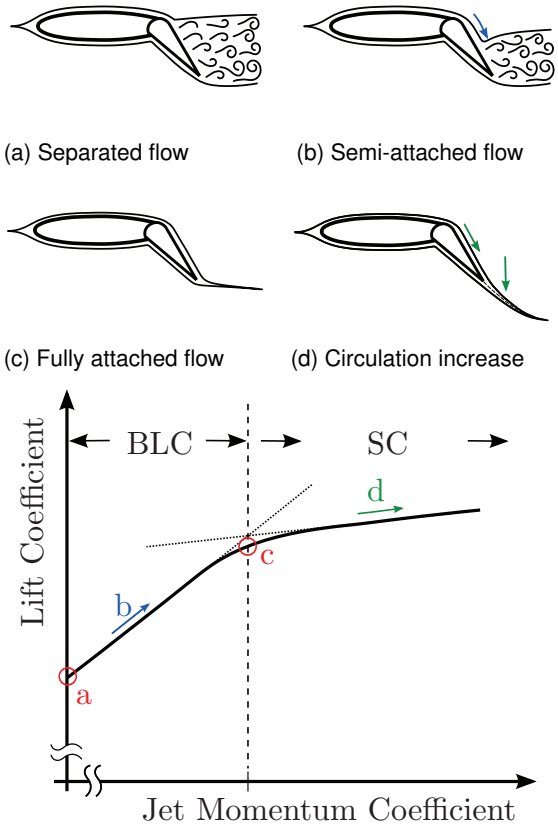

Figure 3: Flow transition for blown flaps

to the flap surface (Figure 3c), additional jet momentum leads to so-called super-circulation (SC), which is less effective than boundary layer control (Figure 3d). The efficiency in lift increase is reflected by the respective gradients in Figure 3e. It is intended to operate the high-lift system at the transition point c, at the border between the two areas. This will be the reference jet momentum in the following. This state appears to be the highest (maximum) lift at optimal blowing efficiency (lift gain factor). The necessary jet momentum to achieve a fully attached airflow depends on the flap deflection. The more a flap is deflected, the more air mass flow is required to prevent the flow from separation.

The wing design is a conservative design with a small leading edge sweep. The top-view sketch in Figure 4 shows the equally distributed six segments with a color coding which shall be used throughout the paper for segment indication. The compressors of segments 1 to 5

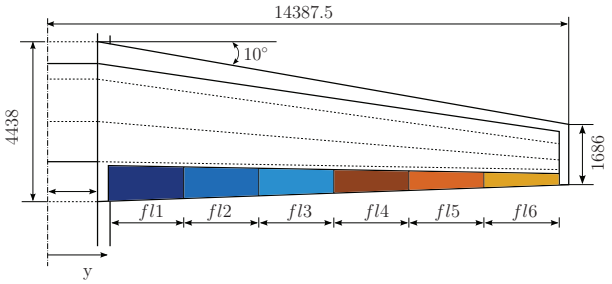

Figure 4: Wing with the six-segmented flap

blow the air over one continuous flap. The segmentation is only referred to the blowing system here. The flap for segment 6 is supposed to have a dual use functionality as high-lift device and roll control surface. In this study the large flap is deflected by $\delta_{fl_{1-5}} = 65°$ and the aileron is drooped by $\delta_{fl_6} = 45°$. This is the full flap setting of the aircraft for the final approach phase and assumed to be fix for this investigation.

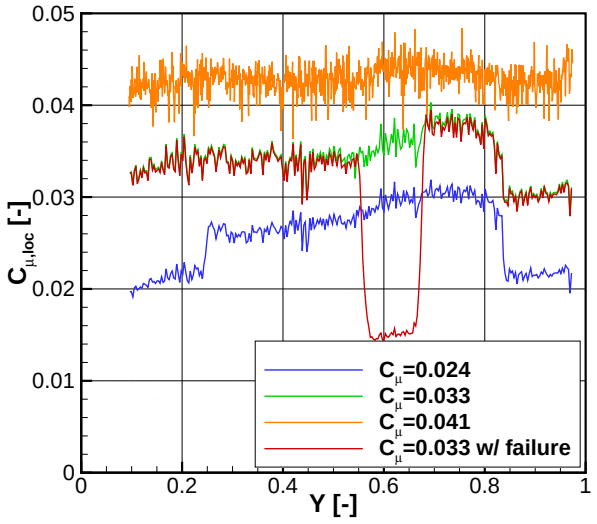

Figure 5: Jet momentum distribution along the blowing slot

3 Aerodynamic Dataset

The aerodynamic dataset of the flight mechanics model is based on numerical simulations, which were performed with the DLR TAU code [17]. For that purpose, 3D simulations of a wing-body model in landing configuration were carried out with a Reynolds Averaged Navier Stokes approach, using the Spalart-Allmaras turbulence model [18] with rotational and curvature correction [19]. In order to simulate the blowing, two separated plena are integrated along the span. The first one combines segments 1 to 5 and is placed in front of the plain flap. The second one is located in front of the aileron and represents segment 6. The plena are pressured by applying a fixed-pressure boundary condition on their endwalls. In order to allow a varying blowing rate along the flap, the flap plenum endwall is separated into its five segments.

Five different cases with varying blowing rates were simulated at a constant angle of attack of $\alpha = 0°$. Besides the case with deactivated blowing ($C_\mu = 0.0$), a case within the boundary layer control area ($C_\mu = 0.024$), one in super-circulation mode ($C_\mu = 0.041$) and one case at the reference blowing rate between boundary layer control and super-circulation ($C_\mu = 0.033$) were simulated. In the fifth case, the blowing rates of all segments except segment 4 are set to the blowing rates of the critical case. The blowing rate of segment 4 is strongly reduced in order to simulate a failure of this segment ($C_\mu = 0.033\,\mathrm{w/failure}$).

Figure 5 depicts the local momentum coefficient distribution along the slot's midline of the four cases with activated blowing. For the case in super-circulation mode, the plenum pressure is kept constant over the span. As a result, the median of the jet momentum coefficient along the span is rather constant, as well. For the other two cases, the plenum pressures are adapted to the local geometry and flow conditions. Besides sweep effects and the deflection angle of the trailing edge device, the local leading edge radius and the local angle of attack are the main drivers, here. Therefore, the jet momentum coefficients steadily increase from the fuselage towards the wing tip until segment 5. The plenum pressure in segment 6 is reduced as the aileron is deflected at a lower angle compared to the flap and therefore needs less blowing. The failure case shows a nearly identical jet momentum coefficient distribution as the reference case, except for segment 4. Here, the local jet momentum coefficient shows a sharp drop, even though the blowing segments are not segregated by walls from each other. The locally reduced blowing rate in the failure case leads to a local flow separation above the flap, as it is visualized in Figure 6.

Behind blowing segment 4, the blowing jet separates from the flap (marked by magenta line), leading to a detached main wing wake and a locally reduced flap suction peak. At the rest of the wing, the flow remains fully attached to the flap and the main wing.

Figure 7 shows the resulting lift distributions, which provide the basis for the flight mechanics model. It shows the distributions along the normalized wingspan Y starting form the centerline of the aircraft. On the inboard side the distributions show the typical disturbances by the fuselage. Due to the circulation control, the lift distributions are significantly shifted towards higher levels, whereas the lift increments in relation to the additional blowing rate are smaller in the super-circulation mode than in the boundary layer control mode. The failure case

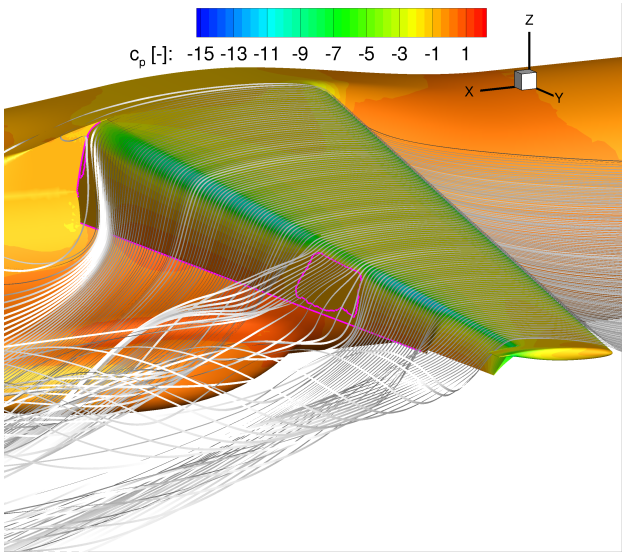

Figure 6: Flow separation in failure case

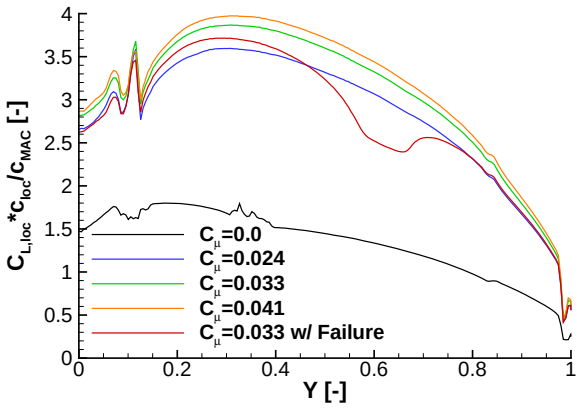

Figure 7: Lift distributions for various blowing rate settings including a segment 4 failure

shows a considerable drop in the local lift at the position of segment 4. However, due to the change in the circulation distribution and the resulting alteration of the locally induced angles of attack, the impact of the failure is not limited to that region. In fact, almost the entire span, from the beginning of the flap to the end of the aileron is negatively affected.

4 Modelling Approach

The overall target for the modeling process is the introduction of lift and rolling moment increments due to spanwise blowing variation to a full flight six degrees of freedom (6-DOF) flight mechanical model. The simulations are performed using MATLAB®/Simulink®[1] which allows a combination of script-based and block diagram modeling.

[1] Release 2007b by Mathworks®

The structure of this model is depicted in Figure 8 showing the force and moment generating sub-systems, which drive the equations of motion. From these equations the resulting aircraft motion is calculated and fed back to the force and moment sub-systems which mostly depend on this motion. The proposed wingspan aerodynamic model is an incremental part of the aerodynamic sub-system. The aerodynamic model is a two-point model approach for the longitudinal motion separating the aerodynamics of the wing/fuselage combination from those of the horizontal tailplane. In the lateral plane a one-point model is used. The wingspan model generates increments for both lateral and longitudinal motion, however the influence of the blowing system on drag and resulting yawing moments will be neglected initially. The model is supposed to leave the capability for fast-time or preferably real-time simulation. Therefore, iterative approaches including aerodynamic calculation methods were not considered. Another reason for this step was the poor capability of simple handbook methods with low computational power consumption to describe such extraordinary aerodynamics, without remarkable adaption effort. It was chosen to find a practical approach with the basic objective to describe fundamental flight mechanical effects. For this purpose the model was based on high-fidelity calculation results serving as sampling points.

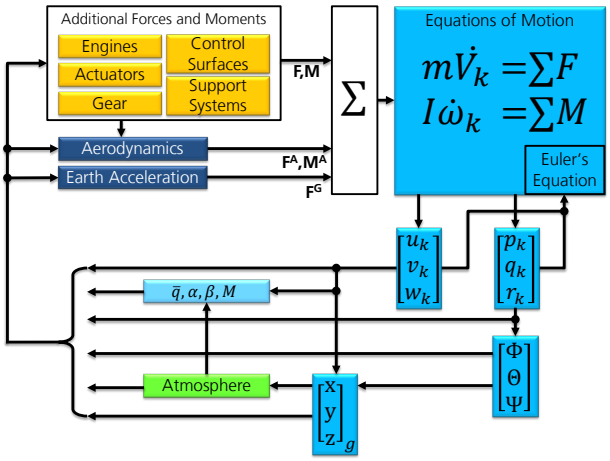

Figure 8: Block diagram showing the model structure of the flight dynamical model [16]

The modeling process is split into two models, the lift distribution due to the setting of the fully functional blowing system and the failure case model. The initial step is the model description of the local lift dC_L, j at each discretization point or strip j along the normalized wingspan Y. Therefore, the gradients between the four known jet momentum states, depicted in Figure 9, have been calculated by:

$$k_{12,j} = \frac{dC_{L,2,j} - dC_{L,1,j}}{C_{\mu,2} - \cancel{C_{\mu,1}}} = \frac{dC_{L,2,j} - dC_{L,1,j}}{C_{\mu,2}} \quad (2)$$

(3) $$k_{23,j} = \frac{dC_{L,3,j} - dC_{L,2,j}}{C_{\mu,3} - C_{\mu,2}}$$

(4) $$k_{34,j} = \frac{dC_{L,4,j} - dC_{L,3,j}}{C_{\mu,4} - C_{\mu,3}}.$$

The resulting lift increment of each discretization step can be calculated by

(5) $$\begin{aligned} dC_{L,j}(C_\mu) = dC_{L,1,j} &+ k_{12,j} \cdot \{C_\mu - \cancel{C_{\mu,1}}\} \\ &+ k_{23,j} \cdot \{C_\mu - C_{\mu,2}\} \\ &+ k_{34,j} \cdot \{C_\mu - C_{\mu,3}\} \end{aligned}$$

with the consideration of different cases $n = 1,2,3,4$ for the jet momentum coefficient

(6) $$\{C_\mu - C_{\mu,n}\} = \begin{cases} 0 & \text{for } C_\mu < C_{\mu,n} \\ (C_\mu - C_{\mu,n}) & \text{for } C_\mu > C_{\mu,n}. \end{cases}$$

These equations relate the lift distribution changes to the

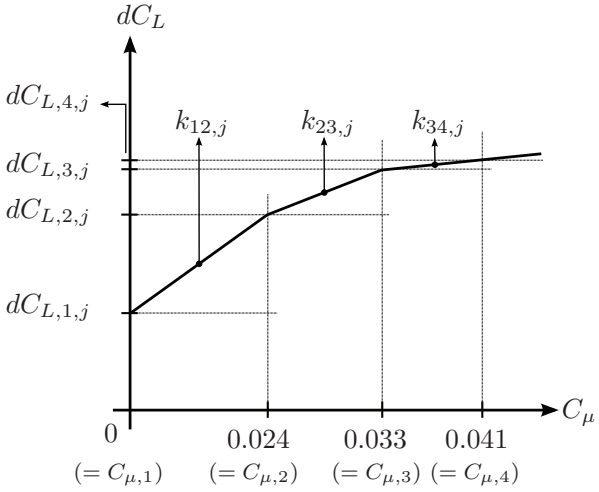

Figure 9: Local lift gradients for global jet momentum coefficient C_μ

global jet momentum C_μ, but since the global jet momentum C_μ is a result of the blowing system setting of each segment, the model has been mapped to the local jet momentum of each segment $C_{\mu,fl,i}$. The local jet momentum is referred to the local airmass flow and the corresponding wing area of each segment i. It is a design parameter of the CFD data and therefore well known. The mapping allows to command a global jet momentum to the submodel, which returns the aerodynamic changes including local settings of each segment. Of course various combinations of local settings can result in the same global jet momentum. The mapping ensures, that the local jet momentum progression fits into the underlying data. Figure 10 shows, how the segment values are calculated by linear interpolation for a commanded jet momentum $C_{\mu,cmd}$ by determination of the mapping gradients $\hat{k}_{12}$, $\hat{k}_{23}$ and $\hat{k}_{34}$ for each segment j. Of course the gradients of

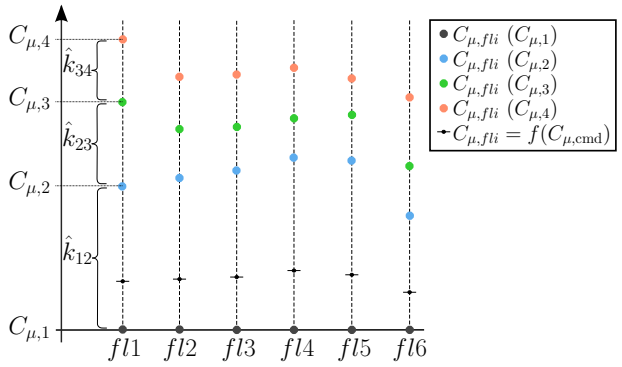

Figure 10: Linear mapping of the global jet momentum to the local segment jet momentum

the Equations (2-4) have been adapted accordingly to the local lift increase of each segment $k_{12,fli,j}$, $k_{23,fli,j}$ and $k_{34,fli,j}$.

A direct outcome of the model is the local rolling moment of each point j by consideration of its corresponding lever arm along the wingspan and the simple calculation

(7) $$dC_{l,j} = dC_{L,j} \cdot Y_j.$$

The further rolling moment modeling is realized analogue to all lift calculations described in the following. Therefore, it is not depicted for better readability preventing redundant explanations.

At this modeling stage, it would be possible to adapt the model such, that each segment could be varied in jet momentum for calculating the resulting lift distributions. However, such a model could not reflect any transition or induced effects exchanged between the segments. Therefore, this part of the model is used solely to describe the distribution changes for the full distribution along the wing. In terms of single segment control the impact along the halfspan is described by a factor model. The approach introduces a failure coefficient E_L, which allows to describe the lift discretization point for a failure by

(8) $$d\tilde{C}_{L,j} = dC_{L,j} \cdot (1 - E_{L,j}).$$

Based on the relation between the difference of the reference ($C_{\mu,3}$) and the complete system shut down case ($C_{\mu,1}$)

(9) $$\Delta dC_{L,13,j} = dC_{L,j}(C_{\mu,3}) - dC_{L,j}(C_{\mu,1})$$

to the segment 4 failure ($C_{\mu,5}$) and the complete system shut down case

(10) $$\Delta dC_{L,15,j} = dC_{L,j}(C_{\mu,5}) - dC_{L,j}(C_{\mu,1})$$

the factor E_L can be described as in

$$E_{L,fl4,j} = 1 - \frac{\Delta dC_{L,15,j}}{\Delta dC_{L,13,j}} \tag{11}$$

for a segment 4 failure as the role model building case.

The failure factor for a segment 4 failure is derived from the underlying CFD data as depicted in Figure 11, which serves as a pattern used to extrapolate the failure behavior for the other segments. Since this is no universal

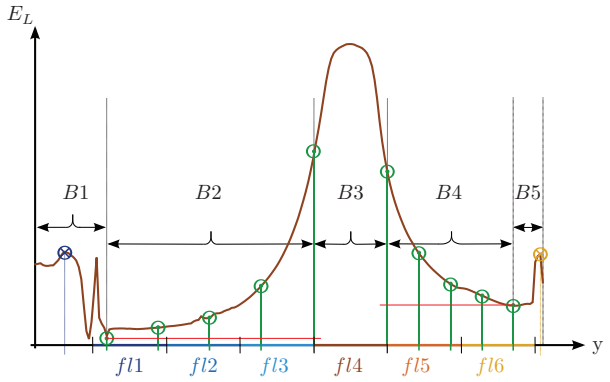

Figure 11: Segment failure factor E_L

approach, the failure factor consists of custom tailored distributions, assuming some restrictions explained in the following. The distributions was split into five areas. The areas $B1$ and $B5$ are fix to keep the boundary conditions. The basic distribution shape in area $B3$ was kept and scaled for the other sections failures. In the areas $B2$ and $B4$ fourth-order polynomials have been fitted to the depicted sampling points (green circles) in order to keep a continuous distribution. Exception are the factor distributions of segment 1 and 6 for which a linear connection to area $B1$ respectively $B5$ was realized. The scaling of the peak shapes for each segment was adapted such, that the sum of all failure factors

$$\sum_{i=1}^{6} (E_{L,fli,j}) = 1 \tag{12}$$

as effectively as possible. This leads to the factor distributions in Figure 12, which also shows the sum of all factors (dashed red line). The final model now can be written as

$$d\tilde{C}_{L,j} = dC_{L,j} \cdot \left(1 - \sum_{i=1}^{6} \left(\kappa_i \cdot E_{L,fli,j}\right)\right). \tag{13}$$

in which κ_i reflects the level of failure from fully operative ($\kappa_i = 0\%$) to total failure ($\kappa_i = 100\%$) for each segment i. This coefficient can be used as a compressor setting control factor under the assumption of a linear behavior, in absence of further sampling points in between.

Certainly the model reliability can be increased by several measures. On the sub-model level, additional data for

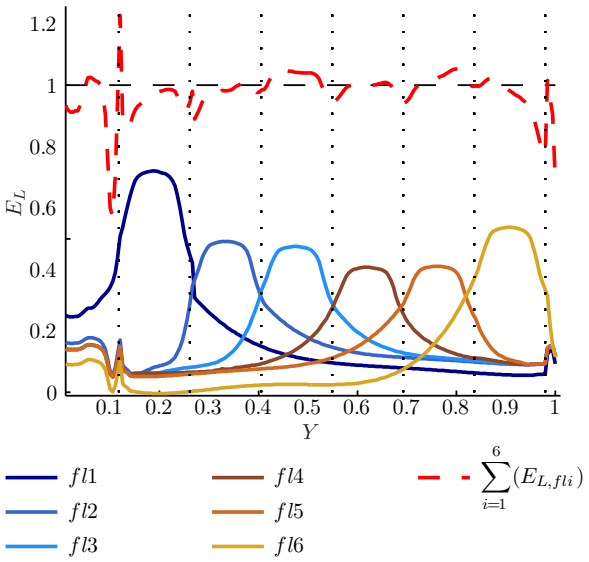

Figure 12: Failure factors for each segment and factor sum

other segment failures can increase the model validity especially of the failure coefficients. A data set with a intermediate blowing setting between failure and reference for one segment can increase the knowledge about the effect evolution for one single segment. On the full wing level, the propeller slipstream also introduces a strong but locally restricted influence on the wing area close to the engines. Hence, another model extension clearly has to be the incorporation of such influence and if viable designed as an incremental model to separate the effects.

5 Performance and Failure Assessment

An initial investigation, which can be performed on this sub-model level is the assessment of counteractions in case of segment failures. Therefore, the target must be to compensate either the lift or rolling moment loss, or even both. For this investigation the simple case to shut down the corresponding segment on the other wing for compensating the rolling moment will not be considered as an option. Instead, it shall be investigated, whether it is possible to compensate at the same wing with reasonable effort. For this purpose the test setup is a compensational jet momentum increase along all remaining operational segments. A failure is calculated for each segment in order to determine the severity of it in terms of effort to counteract. The Figures 13a and 13b show the lift and rolling moment of the fully operative system (green line), compared to the resulting values (blue circles) for each failed segment fli. Moreover, Figure 13a gives the resulting lift due to a full rolling moment compensation

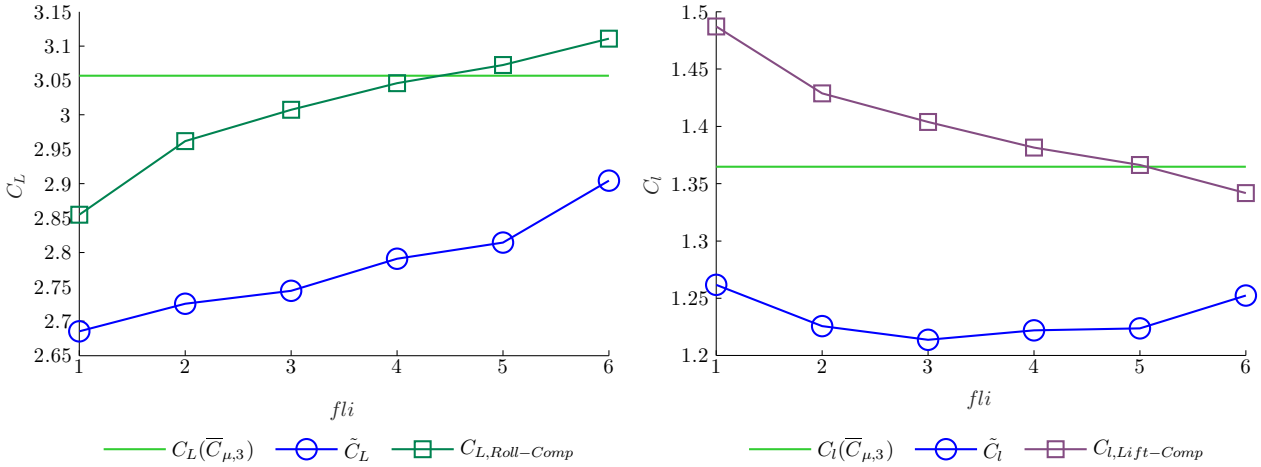

(a) Lift generation due to rolling moment compensation

(b) Rolling moment generation due to lift compensation

Figure 13: Compensation of rolling moment or lift loss

(green boxes). As an example, a failure of flap segment 1 leads to a lift loss below $C_L < 2.7$. A compensation of the corresponding rolling moment increases the remaining lift coefficient to $C_L = 2.85$. Obviously, a full lift compensation cannot be achieved by this compensation method. Accordingly, Figure 13b shows the resulting rolling moment due to a full lift compensation (violet boxes). It is remarkable, that only a compensation of a segment 5 failure is close to a compensation of lift and rolling moment at the same time. For all other cases it is only possible to achieve one of the targets with this setup. It has to be noted that the here used compensation method tries to keep the original shape of the distributions as good as possible with the remaining flap segments.

For different reasons the compensation of the rolling moment appears more reasonable. The relative errors of the non-compensated values emphasize this impression. The values in Table 1 for the remaining lift error during rolling moment compensation ($Error_{L,RC}$) and the rolling moment error during lift compensation ($Error_{l,LC}$) give an indication. According to these results, a rolling moment compensation would cause less relational error in lift, than a lift compensation might cause for the rolling moment. From a pilots perspective, the lift might be increased more easily by angle of attack or airspeed. Therefore, it appears more comfortable than a permanent lateral trimming deflection by the ailerons. Additionally, the necessary compressor settings derived from the investigation underline this suggestion. Figures 14a and 14b show the required performance factors

$$P_{C_\mu,fli} = \frac{C_{\mu,fli,Comp}}{C_{\mu,fli,Ref}} \tag{14}$$

for each compressor during the compensation. According to the introduced color coding, a failure of the corresponding segment leads to significant increases in the performance settings, often multiple times of the original. Especially the lift compensation of a segment 1 failure in Figure 14b is significant, since a performance increase of almost four times would be necessary for compensation with this approach.

This investigation highlights several important aspects. Since the installation space for the compressors is very limited especially at the wing tips, a four times increased performance is more than likely to exceed the compressor's capabilities or forces to accept large ranges of excess power in the compressor design. This will certainly generate unacceptable weight and sizing penalties. From this perspective, a rolling moment compensation appears to be the more feasible choice. However, the chosen setup in terms of increasing the overall performance along the wing neglects, that certain segments might have advantages in the generation of lift or rolling moments. Considering the shape of the lift distributions (Figure 7) a major part of the wings lift is generated in the area of the inner three segments, whereas the outer three segments cover the area of the largest rolling moment contributions to the overall rolling moment (not depicted). It appears reasonable to separate the task of lift and rolling moment compensation and to distribute them to the specialized segments.

Obviously, a segmented wing high lift system offers a wide range of possibilities and scientific questions in terms of control and failure compensation, even on this submodel level. The integration of this model to a full 6-DOF simulation model will even create further interesting fields, as then questions might be answered considering the capabilities of such a system for roll control of the aircraft, while ensuring system safety and of course maintaining high-lift generation.

		$fl1$	$fl2$	$fl3$	$fl4$	$fl5$	$fl6$
$Error_{L,RC}$	$[\%]$	-7.08	-3.21	-1.64	-0.35	-0.5	1.73
$Error_{l,LC}$	$[\%]$	8.24	4.48	2.79	1.21	0.11	-1.71

Table 1: Relative error of the non-compensated values

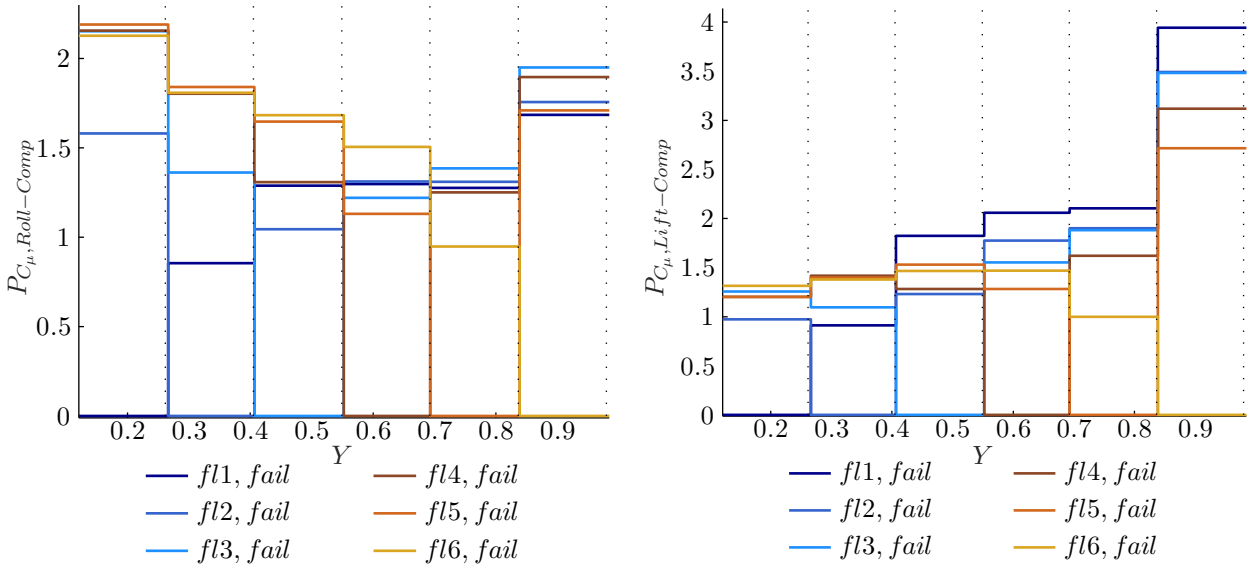

(a) Rolling moment compensation

(b) Lift compensation

Figure 14: Jet momentum performance factor for compensation

6 Conclusions

The presented work shows the development of an increment model for wingspan aerodynamics of a wing with six segments, each equipped with a separate flap blowing system. The focus lies on the capability for fast-time flight dynamics simulation. It's validity is based on the underlying data set, which has been generated with a high-fidelity aerodynamic calculation method employing Reynolds Averaged Navier Stokes equations. The model relates lift and rolling moment to the local segments jet momentum coefficient, which indicates the current performance setting of the segment. For the description of segment failures an additional factor has been introduced, describing the impact of a failure of one single segment on lift and rolling moment of the halfspan of the wing. The factors for each segment have been adapted such, that a failure of all segments automatically describes the aerodynamics of a system shut down, which are known. The failure factor of each segment is scalable from fully operational to total failure. With this modeling approach a good estimation of the flight mechanical behavior of the active high-lift system can be realized. This allows to get a fundamental idea of the influence and potential for control support.

With this model segment failure cases have been assessed on this sub-model level, trying to compensate the lift or rolling moment loss with the remaining operative segments. The results show that a nearly full compensation of both, lift and rolling moment, is only achieved for one failure case. For the other failure cases it appears reasonable to compensate the rolling moment and to correct the remaining lift loss by other measures, such as airspeed or angle of attack increase. However, even a full compensation of the rolling moment can lead to more than a doubling of the necessary jet momentum and thus compressor performance for some failure cases.

The results indicate, that failures of single segments can become a significant factor for aircraft design, in this case especially for the micro-compressor sizing. The current method of increasing all remaining segments to compensate a segment failure can be improved by a more complex control. It is reasonable to assume that some segments are more suited for lift or rolling moment generation, which should be considered for control task assignment. The introduction of drag information along the wingspan and thus yawing moment influences might also be a useful extension of the model. The integration of this sub-model into the full aircraft model will show, if such an active-high lift system can support or even replace a conventional lateral control. Extensive hazard assessments on the full aircraft level have to clarify if a

proper failure and malfunction management is possible.

Acknowledgments

This work has been supported by the provision of particular CFD results for the spanwise aerodynamics of the wing with DLR's TAU code by Dennis Keller. The reference aircraft design has been developed by Wolfgang Heinze[2] with PrADO. The research is conducted within the framework of the Sonderforschungsbereich 880.

References

[1] **B. Norton**, *STOL Progenitors: The Technology Path to a Large STOL Transport and the C-17A* (American Institute of Aeronautics and Astronautics, Reston, VA, USA, 2002)

[2] **J.P. Campbell**, STATUS OF V/STOL RESEARCH AND DEVELOPMENT IN THE UNITED STATES, AIAA Journal of Aircraft, Vol. 1(No. 3), S. 97–106, (1964). AIAA No. 63-482

[3] **R.N. Griffin, C.A. Holzhauser & J.A. Weiberg**, LARGE-SCALE WIND-TUNNEL TESTS OF AN AIRPLANE MODEL WITH AN UNSWEPT, ASPECT-RATIO- 10 WING, TWO PROPELLERS, AND BLOWING FLAPS. Memorandum 12-3-58A, NACA (1958)

[4] **J.A. Weiberg & V.R. Page**, LARGE-SCALE WIND-TUNNEL TESTS OF AN AIRPLANE MODEL WITH AN UNSWEPT, ASPECT-RATIO-10 WING, FOUR PROPELLERS, AND BLOWING FLAPS. Technical Note D-25, NASA (1959)

[5] **J.A. Weiberg & C.A. Holzhauser**, STOL CHARACTERISTICS OF A PROPELLER-DRIVEN, ASPECTRATIO-10, STRAIGHT-WING AIRPLANE WITH BOUNDARYLAYER CONTROL FLAPS, AS ESTIMATED FROM LARGESCALE WIND-TUNNEL TESTS. Technical Note D-1032, NASA (1961)

[6] **T. Dansby, W.C.J. Garrard, D.M. Ryle & L.J. Sullivan**, V/STOL DEVELOPMENT OF THE C-130 HERCULES, AIAA Journal of Aircraft, Vol. 1(No. 5), S. 242–252, (1964)

[7] **H.C. Quigley & R.C. Innis**, HANDLING QUALITIES AND OPERATIONAL PROBLEMS OF A LARGE FOUR-PROPELLER STOL AIRPLANE. Technical Note D-1647, NASA (1963)

[8] **H.C. Quigley & H.F. Lawson**, SIMULATOR STUDY OF THE LATERAL-DIRECTIONAL HANDLING QUALITIES OF A LARGE FOUR-PROPELLERED STOL TRANSPORT AIRPLANE. Technical Note D-1773, NASA (1963)

[9] **C. Werner-Westphal, W. Heinze & P. Horst**, Multidisciplinary Integrated Preliminary Design Applied to Future Green Aircraft Configurations, in *45th AIAA Aerospace Sciences Meeting and Exhibit* (American Institute of Aeronautics and Astronautics, 2007). DOI 10.2514/6.2007-655

[10] **S. Teichel, M. Dörbaum, O. Misir, A. Merkert, A. Mertens, J.R. Seume & B. Ponick**, Design considerations for the components of electrically powered active high-lift systems in civil aircraft, CEAS Aeronautical Journal, Vol. 6, S. 49 – 67, (2014)

[11] **J.R. Seume, S. Teichel, M. Burnazzi, M. Schwerter, C. Behr, A. Rudenko, A. Schmitz, M. Dörbaum & C. Atalayer**, SFB 880 - Efficient Flight. Proceedings of the 62nd Deutscher Luft- und Raumfahrtkongress 2013 (2013)

[12] **S. Sakurai, S. Fox, K. Beyer, D. Lacy, P. Johnson, S. Wells, J. Noble, P. Meredith, N. Huynh, R. Christianson et al.**, Multi-function trailing edge devices and associated methods (2005). US Patent 2005/0011994 App. 10/860,438

[13] **M. Burnazzi & R. Radespiel**, Design and analysis of a droop nose for coanda flap applications, Journal of Aircraft, Vol. 51(No. 5), S. 1567–1579, (2014). DOI 10.2514/1.C032434

[14] **M. Burnazzi & R. Radespiel**, Synergies between suction and blowing for active high-lift flaps, CEAS Aeronautical Journal, Vol. 6(Iss. 2), S. 305 – 318, (2015). DOI 10.1007/s13272-014-0146-8

[15] **D. Keller & R. Rudnik**, Integration Aspects of Lift Augmentation Systems on the Aerodynamics of a High-Lift Configuration, in *SFB 880 - Fundamentals of high-lift for future commertial aircraft, Biennial Report*, (Hrsg.) **R. Radespiel & R. Semaan** (TU Braunschweig - Campus Forschungsflughafen, Braunschweig, 2015), S. 145–156

[16] **J.H. Diekmann & K.U. Hahn**, Effect of an active high-lift system failure during landing approaches, CEAS Aeronautical Journal, Vol. 6(Issue 2), S. 181–196, (2015). DOI 10.1007/s13272-014-0139-7

[17] **T. Gerhold**, Overview of the Hybrid RANS Code TAU, in *MEGAFLOW – Numerical Flow Simulation for Aircraft Design*, *Notes on Numerical Fluid Mechanics and Multidisciplinary Design*, Vol. 89, (Hrsg.) **N. Kroll & J. Fassbender** (Springer, 2005), S. 81–92

[18] **P. Spalart & S. Allmaras**, A One–Equation Turbulence Model for Aerodynamic–Flows, in *30th Aerospace Sciences Meeting and Exhibit*, 92–0439 (AIAA, 1992)

[2] Institute of Aircraft Design and Lightweight Structures (IFL), TU Braunschweig

[19] **P. Spalart & M. Shur**, On the sensitization of turbulence models to rotation and curvature, Aerospace Science and Technology, 1(Issue 5), S. 297–302, (1997)